International Journal of Thermal Technologies
E-ISSN 2277 – 4114

Available at http://inpressco.com/category/ijtt/

Research Article

Effective numerical model for flow boiling of a nanofluid

Anurag Alam Shetty[#], Pradyumna Ghosh[#*], S.S.Mondal[#], Nirupama Patra[^] and R.S.Singh[^]

[#]Department of Mechanical Engineering, Indian Institute of Technology (BHU), Varanasi-221005, UP, India
[^]Department of Chemical Engineering, Indian Institute of Technology (BHU), Varanasi-221005, UP, India

Received 01 April, Accepted 01 June 2017, Available online 05 June 2017, **Vol.7, No.2 (June 2017)**

Abstract

Flow boiling of Al_2O_3-Water nanofluid has been investigated numerically using the Eulerian multiphase model in ANSYS FLUENT. The physical properties have been computed using the two phase mixture model. In the Eulerian multiphase model, Rensselaer Polytechnic Initiative (RPI) nucleate boiling model has been used for modeling boiling. Axial vapor fraction has been computed in case of flow boiling of water and heat transfer coefficient has been computed in case of flow boiling of Al_2O_3-Water nanofluid. The numerical results obtained were in good agreement with experimental results. The RPI model predicts the heat transfer characteristics quickly.

Keywords: *Keywords: Nanofluid, Flow boiling, RPI modeling, FLUENT*

Nomenclature

ρ_q	Phase reference density	V_d	Volume of bubble on departure
α_q	Volume fraction of phase q	N_w	Active nucleation site density
$\dot{m}_{pq}$	Mass transfer from p to q	ρ_v	Vapor density
K_{pq}	Interphase momentum exchange coefficient	$\dot{m}_{l\to v}$	Mass transfer rate from liquid phase to vapor phase
μ_q	Shear viscosity of phase q	$\dot{m}_{v\to l}$	Mass transfer rate from vapor phase to liquid phase
λ_q	Bulk viscosity of phase q	h_{fv}	Latent heat of evaporation
$\vec{F}_q$	External body force	f	Frequency of bubble departure
$\vec{F}_{lift,q}$	Lift force	$\vec{V}_v$	Vapor phase velocity
$\vec{F}_{vm,q}$	Virtual mass force	ϕ	Volume fraction of nanoparticles
h_q	Specific enthalpy	ρ_{nf}	Density of nanofluid
S_q	Source term	ρ_{bf}	Density of base fluid
Q_{pq}	Intensity of heat exchange	ρ_p	Density of nanoparticle
h_{pq}	Interphase enthalpy	$c_{p_{nf}}$	Specific heat capacity of nanofluid
h_C	Single phase heat transfer coefficient	$c_{p_{bf}}$	Specific heat capacity of base fluid
T_w	Temperature of the wall	c_{p_p}	Specific heat capacity of nanoparticle
T_l	Temperature of the liquid	k_{nf}	Thermal conductivity of nanofluid
λ_l	Thermal diffusivity of liquid	k_p	Thermal conductivity of nanoparticle
k_l	Thermal conductivity of liquid	k_{bf}	Thermal conductivity of base fluid
θ	Angle of contact	f	Drag
d_p	Diameter of bubble of phase p	τ_p	Particulate relaxation time
A_i	Interfacial area	S_k	Turbulent kinetic energy
v_{fg}	Difference in specific density of liquid and vapor	S_ε	Turbulent dissipation rate

1. Introduction

Cooling is one of the key parameters in maintaining the required reliability of high heat dissipation density heat transfer device, ranging from nuclear reactor core to various miniaturized electronic components. Nanofluids are homogeneous fluid mixtures which can play a significant role in satisfying these cooling requirements. A nanofluid is basically a colloidal solution of nano sized particles in a base fluid. Demir et al reported that despite being a two phase in reality, nanofluids show behavior of pure fluid. Introduction of nanoparticles into a base fluid has significant effect on the thermo-physical properties such as density, specific heat, thermal conductivity, enthalpy of evaporation and viscosity. Corcion investigated various experimental results of nanofluids containing nanoparticles such as alumina, copper oxide and titanium dioxide against empirical correlations. Substantial increase in both thermal conductivity and viscosity were reported. Tso et al. reported variation in the evaporation enthalpy of water based nanofluids of Al_2O_3 and TiO_2 for various concentrations.

One of the most important parameters in cooling applications is the heat transfer coefficient. Kim et al. did extensive experimental investigation on the heat transfer coefficient in a vertical tube at high mass flux and very high wall heat fluxes. They investigated for

*Corresponding author's ORCID ID: 0000-0003-0926-2974;
DOI: http://dx.doi.org/10.14741/ijtt.v7i.8275

low concentrations of alumina, zinc oxide and diamond nanoparticles in water at atmospheric pressure. Another important characteristic of the flow boiling is the void fraction. The void fraction decides the flow regime and the stability of the flow. For example, transition into film boiling has adverse effects on the heat transfer characteristics. Lee et al. investigated the axial and radial profiles of void fraction in vertically inner heated annulus for subcooled flow boiling of water.

Various numerical studies have been conducted by researchers for both base fluids and nanofluids using single phase and two phase approach. Two phase approach has been implemented using mostly three different methods; mixture methods, Eulerian-Eulerian method and Eulerian-Lagrangian method. Aabrajith and Dhir studied the effect of contact angle on growth and departure of a single bubble on a horizontal heated surface for atmospheric conditions. They found that in general, lower the contact angle, smaller the bubble departure diameter and the growth period. Li et al. numerically investigated the flow boiling of nitrogen in a vertical tube using the two fluid model. Koncar and Mavko numerically modeled subcooled flow boiling of water using the system code RELAP5 while similar work was done by Tu and Yeoh in the Computation Fluid Dynamics code CFX.

Abedini et al. modeled the nanofluid as a single phase using CFX solver considering Mixture model. They implemented the nanofluid properties by implementing the effective viscosity and specific heat capacity to calculate the effective heat transfer coefficient. They concluded that increase in nanoparticle concentration increases the rate of heat transfer. Aminfar et al. used both the single phase and two phase model for modeling of nanofluid using the Mixture model along with wall heat flux partitioning at the walls. They noted that there is not much difference between the results of the proposed two phases and three phases method and both were in agreement with both the experimental results and the correlations.

In the present investigation, the Eulerian multiphase model along with wall heat flux partitioning has been used for computation of void fraction for flow boiling of water and for heat transfer coefficient in flow boiling of low concentrations (0.1%, 0.01% and 0.001%) of Al_2O_3 nanoparticles in water. Eulerian models have been implemented using the commercial CFD code ANSYS FLUENT as no comprehensive studies are available which model will be applicable for quick engineering heat transfer calculation.

2. Mathematical modeling

Eulerian Multiphase

The wall boiling model implemented is present within the general Eulerian multiphase framework of ANSYS FLUENT. In this model, momentum and continuity equations are solved for each individual phase. All the phases in this model share the same pressure equation, i.e. for separate momentum and continuity equations, a single pressure equation is solved for all the phases (M. Flows). Furthermore, $k-\varepsilon$ $(k-Epsilon)$ turbulence model has been implemented (M. Flows). These general equations have not been discussed for brevity. This model was used for simulating the vapor fraction in case of pure water and wall heat transfer coefficient in case of Al_2O_3/Water nanofluids.

The wall boiling phenomenon has been modeled by RPI nucleate boiling model (N. Kurul et al, 1991). Sub models have been used to account for interfacial transfer of momentum heat and mass.

RPI Nucleate boiling model

Kurul and Podowski proposed a boiling model which partitions the heat transfer from the surface into three categories to account for convection, quenching and evaporation. The Eulerian multiphase model in ANSYS FLUENT incorporates wall boiling models which can be used for subcooled boiling.

As per the basic RPI model, the total heat flux transferred from the surface was transmitted in three parts, namely, convective heat flux, the quenching heat flux and the evaporation heat flux.

$$\dot{q}_W = \dot{q}_C + \dot{q}_Q + \dot{q}_E \tag{1}$$

The area of the heated wall is divided into two parts, A_b, the area covered with nucleating bubbles and the region exposed to the liquid phase, $(1-A_b)$ which is covered by the liquid.

$$\dot{q}_C = h_C(T_w - T_l)(1-A_b) \tag{2}$$

The quenching heat flux $\dot{q}_Q$ is computed by cyclic average of the heat transferred to the liquid filling the vicinity of the region departed by the bubble and is expressed as:

$$\dot{q}_Q = \frac{2k_l}{\sqrt{\pi\lambda_l T}}(T_w - T_l) \tag{3}$$

Where T is the periodic time

The evaporative heat flux $\dot{q}_E$is given by:

$$\dot{q}_E = V_d N_w \rho_v h_{fv} f \tag{4}$$

Area of influence

The area of the heater surface covered by nucleating bubbles,A_b, also known as the area of influence is given by:

$$A_b = min(1, K\frac{N_w \pi D_w^2}{4}) \tag{5}$$

The value of empirical constant K may vary between 1.8 and 5. Del Valle and Kenning proposed the following relation for a more accurate determination of the constant K.

$h_{sl} = \frac{k_l}{D_b}(2 + 0.6Re^{0.5}Pr^{0.33})$ ()
$K = 4.8e(-Ja_{sub}/80)$ (6)

And Ja_{sub} is the subcooled Jacob number which is defined as:

$$Ja_{sub} = \frac{\rho_l C_{pl} \Delta T_{sub}}{\rho_v h_{fv}} \quad (7)$$

Where, $\Delta T = T_{sat} - T_l$.

Frequency of bubble departure

The frequency of bubble departure is based on the correlation suggested by Cole. It is based on the inertial controlled growth of the bubble.

$$f = \frac{1}{\mathrm{T}} = \sqrt{\frac{4g(\rho_l - \rho_v)}{3\rho_l D_w}} \quad (8)$$

Nucleate site density

The nucleate site density is expressed as a function of wall superheat. Its general form is:

$$N_w = C^n(T_w - T_{sat})^n \quad (9)$$

The empirical parameters of the equation are used as proposed by Lemmert and Chawla. Based on their findings $n = 1.805$ and $C = 210$.

Bubble departure diameter

The default bubble departure diameter in this model is based on the correlation by Tolubinsky and Kostanchuk. It is calculated in millimeters as:

$$D_w = \min(0.0014, 0.0006e^{-\frac{\Delta T_W}{45.0}}) \quad (10)$$

Interfacial transfers

Interfacial area

Interfacial drag and interfacial heat transfer depend on the interfacial area. Due to the coalescence of bubbles in the domain, bubble diameter cannot be considered for calculation of interfacial drag and heat transfer. The particle model was used in this case:

$$A_i = \frac{6\alpha_v}{D_b} \quad (11)$$

Interfacial momentum transfer

Interfacial momentum transfer includes drag, lift and turbulent drift forces.

Interfacial drag force

The momentum exchange coefficient between two phases is based on the value of exchange coefficient K_{pq}. Its general form is given by:

$$K_{pq} = \frac{\alpha_q \alpha_p \rho_p f}{\tau_p} \quad (12)$$

$$\tau_p = \frac{\rho_p d_p^2}{18\mu_q} \quad (13)$$

The drag function, f, was computed using the model of Schiller and Naumann.

$$f = C_D Re/24 \quad (14)$$

$$C_D = \begin{cases} 24(1 + 0.15Re^{0.687})/Re, & Re \le 1000 \\ 0.44, & Re > 1000 \end{cases} \quad (15)$$

$Re$is the relative Reynolds number. Re for primary phase p and secondary phase q is given by:

$$Re = \frac{\rho_q |\vec{v}_p - \vec{v}_q| d_p}{\mu_q} \quad (16)$$

Interfacial lift force

The correlation proposed by Moraga et al. has been used for calculation of coefficient of interfacial lift.

$$C_{Lift} = \begin{cases} 0.00767, & \varphi > 6000 \\ -\left(0.12 - 0.2^{-\frac{\varphi}{3600}}\right)^{\frac{\varphi}{e^3}\times 10^{-7}}, & 6000 \le \varphi \le 1.9 \times 10^5 \\ -0.002, & \varphi < 1.9 \times 10^5 \end{cases} \quad (17)$$

Where,$\varphi = Re_b Re_v$

The lift coefficient combines the effect of classical aerodynamics lift force resulting from bubble and liquid shear and the lateral force due to interaction between bubble and the wake generated behind the bubble. The bubble Reynolds number, $Re_b = \frac{D_b \rho_l |V_l - V_v|}{\mu_l}$ and the bubble shear Reynolds number, $Re_v = \frac{D_b^2 \rho_l (\nabla V_l)}{\mu_l}$.

Turbulent drift force

The turbulent drift force is based on the model suggested by Simonin. It is given by:

$$\overrightarrow{F_{lv}}^{TD} = -\overrightarrow{F_{vl}}^{TD} = -C_{TD}\rho_l k \nabla \alpha_v \quad (18)$$

Where, k is the turbulent kinetic energy and C_{TD} is the turbulent dispersion coefficient. It is set to 1 by default.

Interfacial heat transfer

Interface to liquid heat transfer

The heat transfer from the bubble to the liquid is defined as:

$$\dot{q}_{lt} = A_i h_{sl}(T_{sat} - T_l) \quad (19)$$

Here A_i is the interfacial area and h_{sl} is the heat transfer coefficient given by Ranz-Marshall correlation.

$$h_{sl} = \frac{k_l}{D_b}(2 + 0.6Re^{0.5}Pr^{0.33}) \quad (20)$$

Interface to vapor heat transfer

Constant time scale return to saturation method is used to calculate the interface to vapor heat transfer. In this method it is assumed that the vapor retains its saturation temperature by rapid evaporation and condensation.

$$\dot{q}_{vt} = \frac{\alpha_v \rho_v C_{p,v}}{\delta t}(T_{sat} - T_v) \quad (21)$$

Where δ_t is set to a default value of 0.05 and $C_{p,v}$is the isobaric heat capacity.

Mass transfer

Mass transfer from wall to vapor

Evaporation heat flux is used to compute the evaporation mass flow at the cells near the wall.

$$\dot{m}_E = \frac{\dot{q}_E}{h_{fv} + C_{p,l}\Delta T_{sub}} \quad (22)$$

Interfacial mass transfer

Interfacial mass transfer is computed based on the assumption that all heat transferred to the interface is used in mass transfer. It can be written as:

$$\dot{m} = \dot{m}_{lt} + \dot{m}_{vl} = \frac{\dot{q}_{lt} + \dot{q}_{vt}}{h_{fv}} \quad (23)$$

Turbulence models

For $k - epsilon$ models, additional terms have been included to account for bubble stirring and dissipation. One of the terms is included in turbulent kinetic energy (S_k), and other in turbulent dissipation rate (S_ε):

$$S_k = \frac{3}{4}\frac{\alpha_v(1-\alpha_v)\rho_l C_D}{D_b}\left|\vec{V}_l - \vec{V}_v\right|^2 \quad (24)$$

$$S_\varepsilon = C_{\varepsilon 3}\frac{3C_D}{D_b}\left|\vec{V}_l - \vec{V}_v\right|S_k \quad (25)$$

Here $C_{\varepsilon 3} = 0.45$ as per Troshko et al..

Incorporation of nanofluid properties

In order to simulate the flow boiling of nanofluids the properties of nanofluids were introduced in the predefined model using the following:

Density

Volume fraction averaged density was computed using the following equation:

$$\rho_{nf} = \rho_{bf}(1 - \phi) + \rho_p\phi \quad (26)$$

Specific heat capacity

The specific heat capacity was computed similar to density but the effect of density was incorporated:

$$c_{p_{nf}} = \frac{\rho_{bf}c_{p_{bf}}(1-\phi) + \rho_p c_{p_p}\phi}{\rho_{bf}(1-\phi) + \rho_p\phi} \quad (27)$$

Viscosity

In the Eulerian multiphase model, the viscosity of the nanofluid was computed as per the correlation proposed by Maiga et al.

$$\mu_{nf} = (123\phi^2 + 7.3\phi + 1)\mu_{bf} \quad (28)$$

In the Volume of fluid model, the viscosity of the nanofluid was computed as per the correlation proposed by H. Brinkman.

$$\mu_{nf} = \frac{\mu_{bf}}{(1-\phi)^{2.5}} \quad (29)$$

Thermal conductivity

The thermal conductivity of the nanofluid was computed as per the Maxwell equation.

$$\frac{k_{nf}}{k_{bf}} = \frac{(k_p + 2k_{bf}) - 2\phi(k_{bf} - k_p)}{(k_p + 2k_{bf}) + \phi(k_{bf} - k_p)}$$

For the case when Brownian motion was considered, the thermal conductivity relation developed by Koo & Kleinstreuer was used.

$$k_{nf} = k_f + 3\varphi\frac{k_p - k_f}{2k_f + k_p - \varphi(k_p - k_f)}k_f + 5 \times 10^4\beta\rho_f C_f\varphi\sqrt{\frac{k_b T}{2\rho_p r_p}}\left[(-134.63 + 1722.3\varphi) + (0.4705 - 6.04\varphi)T\right] \quad (30)$$

The parameter β is related to the nanoparticle Brownian motion and was determined empirically as

$$\beta = 0.0137(100\,\varphi)^{-0.8229}, for\ \varphi < 0.01 \quad (31)$$

$$\beta = 0.0011(100\,\varphi)^{-0.7272}, for\ \varphi > 0.01$$

Surface tension

The surface tension was computed as per the proposed equation by Vargaftik et al.

$$\sigma = B\left[\frac{T_C - T}{T_c}\right]^a\left[1 + b\left[\frac{T_C - T}{T_C}\right]\right] \quad (32)$$

Where,

$B = 235.8 \times 10^{-3} N/m$
$a = 1.256$
$T_c = 647.15K$

Enthalpy of evaporation

The enthalpy of evaporation for different nanofluids was taken from the findings of Tso et al.. Since in ANSYS FLUENT, neither VOF nor Eulerian multiphase model have a direct method of incorporating the enthalpy of evaporation, it was done so by appropriately modifying the Standard State Enthalpy of water.

3. Numerical modeling

Three sets of simulations were performed on two different axisymmetric domains, using the Eulerian multiphase model. Eulerian multiphase model was used to compute vapor fraction for annular flow of water and validated against the experimental observations of Cheung et al.. They performed flow boiling of water in a vertical annular pipe with heated inner tube of 12.7mm diameter and outer wall of diameter 25.4mm. The experimental section was 306mm long. A 6x306 cell mesh was used to simulate the computation domain of 6.35mm×306mm. The domain was an axisymmetric domain of 3.175mm ×100mm meshed as a grid of 6 × 20. Mesh independent study has been carried out within 3.2 % fluctuation in the results. The test conditions which were simulated in this model are listed in table1.

Table 1: Numerical test conditions

$Case$	$P_{inlet}(MPa)$	$T_{inlet}(°C)$	$T_{sub}(inlet)(°C)$	$Q_w(kW/m^2)$	$G(kg/m^2s)$
1	0.137	91.9	14.9	286.7	156.2
2	0.122	93.6	11.6	286.5	258.2
3	0.150	94.6	16.6	508.0	264.3
4	0.150	88.9	22.5	705.0	411.7

Table 2: Thermo-physical Properties of Alumina Nanofluid

$Concentration\ v/vby$ %	$Density\ kg/m^3$	$Viscosity\ kg/ms$	$Thermal\ conductivity\ W/mK$	$Specific\ heat\ J/kgK$
0	998.2	0.00089	0.6	4182
0.001	998.23	0.000890065	0.605	4181.87
0.01	998.49	0.000890651	0.605	4180.69
0.1	1001.17	0.0008966	0.6067	4168.9

Due to the almost incompressible nature of flow in the present case, a pressure based solver is used. A coupled solver has the advantage of being more robust as it solves the momentum and pressure correction equations together. Furthermore, in case of large mesh size and steady flows a coupled solver is more stable. Therefore, in this model a coupled solver is used.

The flow boiling of Al_2O_3/Water nanofluid was simulated using both the Eulerian Multiphase model and the VOF model. The Eulerian Multiphase model was used to compute the heat transfer coefficient. The domain for the Eulerian multiphase model consists of a vertical heated steel tube of OD 6.35 mm and thickness 0.41 mm. The domain is simulated in ANSYS FLUENT using an axisymmetric assumption. The simulation was performed for Al_2O_3/Water nanofluids concentration of 0.1%, 0.01% and 0.001% by volume.

The calculated physical properties for them are listed in table 2.

The surface tension of nanofluid was considered same as water and was considered as a function of temperature given by equation (33). The unit is N/m

$$S = -3 \times 10^{-7}T^2 - 2 \times 10^{-6}T + 0.0955 \qquad (33)$$

The simulated test conditions are tabulated in table 3.

Table 3a: Operating conditions for numerical experiment

$Velocity\ (m/s)$	$Heat\ flux\ (MW/m^2)$	$T_{inlet}(K)$
2.5	0.5, 1.0, 1.5, 2.0 *and* 2.5	353
2.0	0.5, 1.0, 1.5 *and* 2.0	353
1.5	0.5, 1.0 *and* 1.5	353

The VOF model was used to simulate the bubble development and departure in a tube of diameter 15mm and length 600mm. An axisymmetric mesh of 7.5mm × 600mm was simulated using a grid of 50 × 4000.

Table 3b: Operating conditions for numerical experiment for VOF model

$Concentration\ v/vby$ %	$Velocity\ m/s$	$Heat\ flux\ kW/m^2$	$T_{inlet}\ K$
1	0.01	10	373

The time step used was $2x10^{-6}$s. The PISO (Pressure Implicit with Splitting of Operators) scheme, an extension of SIMPLE algorithm was used as the pressure-velocity coupling.

4. Results and discussions

For verification and validation purpose comparisons have been made of the CFD solution comparisons have

been made. In case of the Eulerian multiphase model the numerical results were compared experimental findings of Cheung et al. for base fluid and Kim et al. for the various concentrations of Al_2O_3/Water nanofluids.

4.1: Void fraction

For water

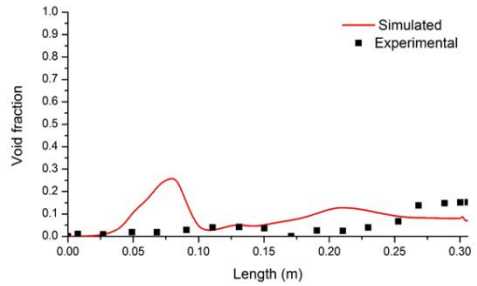

Figure 1: Axial vapor fraction v/s length for Case I

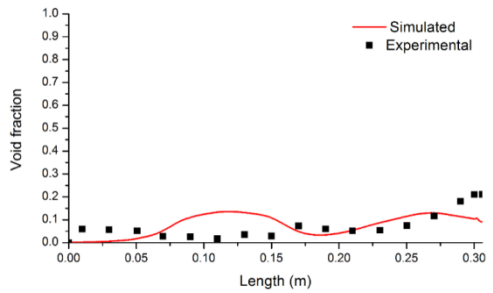

Figure 2: Axial vapor fraction v/s length for Case II

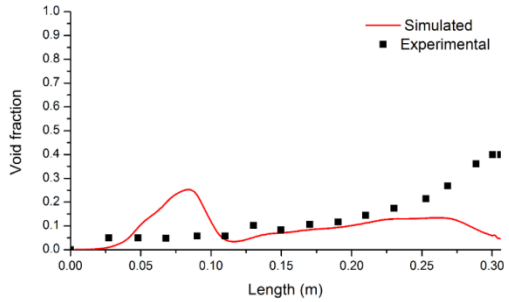

Figure 3: Axial vapor fraction v/s length for Case III

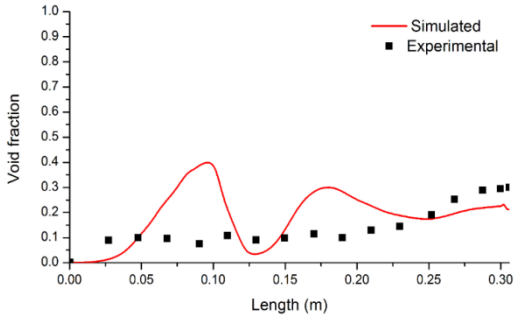

Figure 4: Axial vapor fraction v/s length for Case IV

In the flow boiling of water, as can be observed in figures 1,2,3 and 4, the simulated axial void fraction was not in very good agreement with the experimental void fraction. However, the deviation in the void fraction was not greater than ±0.2. Furthermore, the maximum axial void fraction computed by the simulation was in agreement with the maximum void fraction obtained in the experiment. A significant drop in axial void fraction at the end of the tube was observed in Cases 1, 2 and 3. This can be attributed to the fact that only the inlet conditions to the model were known, while the outlet pressure was set to 101.325 kPa for all of the cases. It may be possible to obtain results with higher accuracy if the outlet conditions are known.

4.2: Heat transfer coefficient

For Al_2O_3/Water nanofluid

For the Eulerian multiphase model, the comparison of the simulation results with the experimental results by Kim *et al.* has been done using figures 6-14. The heat transfer coefficient has been computed using the inlet temperature as the bulk temperature.

For $Inlet\ velocity = 2.5\ m/s$

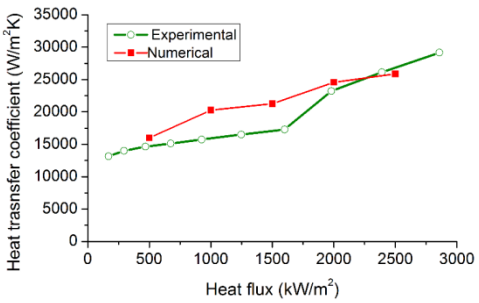

Figure 4: Heat transfer coefficient for water

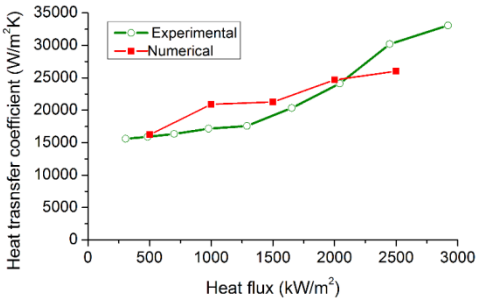

Figure 5: Heat transfer coefficient for 0.1% v/v Al_2O_3.

In case of flow boiling of Al_2O_3/Water nanofluid, as shown in figures (6-8) the simulated heat transfer coefficient exhibited a deviation of about 25% in case of velocity of 2.5m/s. The model was over predicting the heat transfer coefficient in lower heat fluxes and under predicting at high heat fluxes. At relatively lower velocities of 2.0m/s and 1.5m/s, the model was not stable at higher heat fluxes. Furthermore, in these cases the heat transfer coefficient was over predicted for lower heat fluxes. This over prediction of heat transfer coefficient can be attributed to the reason that the bulk temperature of the flow was considered to be

same as that at the inlet, thereby not accounting for the sensible heating the bulk fluid.

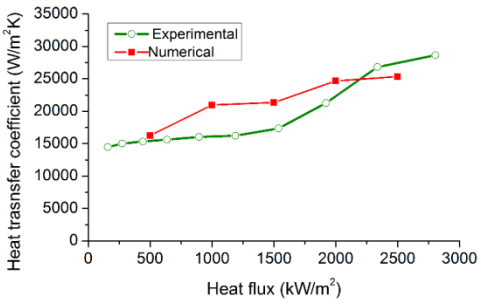

Figure 6: Heat transfer coefficient for 0.01% v/v Al_2O_3

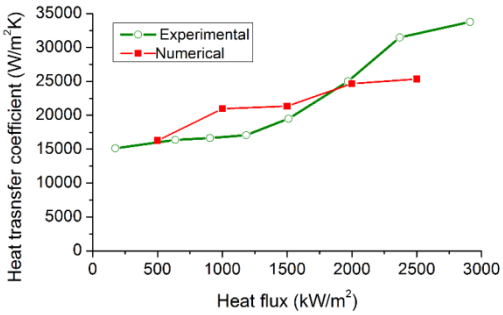

Figure 7: Heat transfer coefficient for 0.001% v/v Al_2O_3

For *Inlet velocity* = 2.0 m/s, at various concentration of nanofluid heat transfer coefficients have been plotted in figures (9-10).

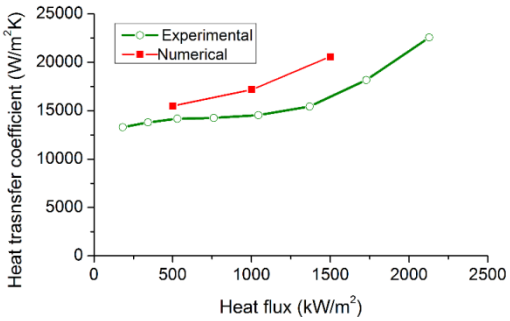

Figure 8: Heat transfer coefficient for water

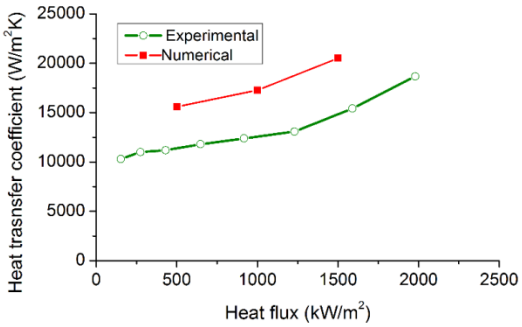

Figure 9: Heat transfer coefficient for 0.1% v/v Al_2O_3

For *Inlet velocity* = 1.5 m/s, at various concentration of nanofluid heat transfer coefficients have been plotted in figures (11-12). However, figures indicate the model is applicable for higher inlet velocity of 2.5 m/s for descent prediction and the differences with experimental and CFD results differs significantly in case of lower velocity.

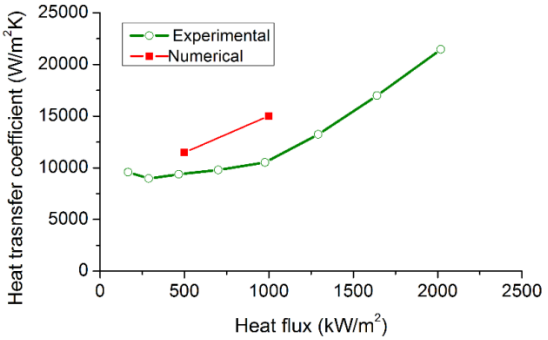

Figure 10: Heat transfer coefficient for water

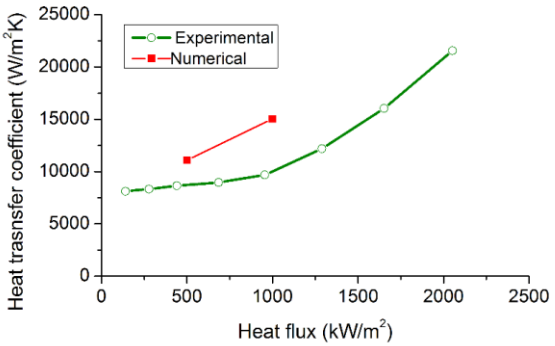

Figure 112: Heat transfer coefficient for 0.1% v/v Al_2O_3

The comparison of heat transfer coefficient of flow boiling of water and nanofluid is done in the next six graphs, figures (13-18).

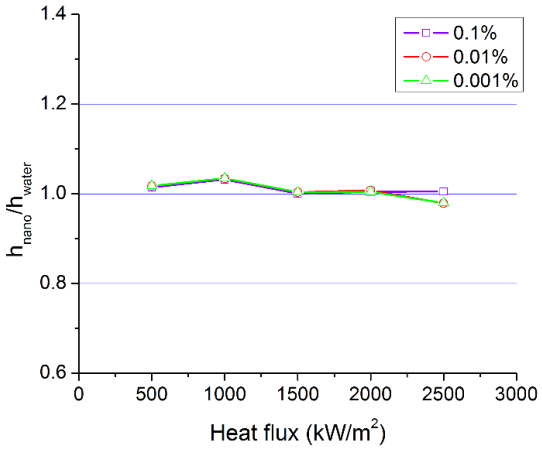

Figure 123: h_{nano}/h_{water} for inlet velocity = 2.5 m/s.(Numerical)

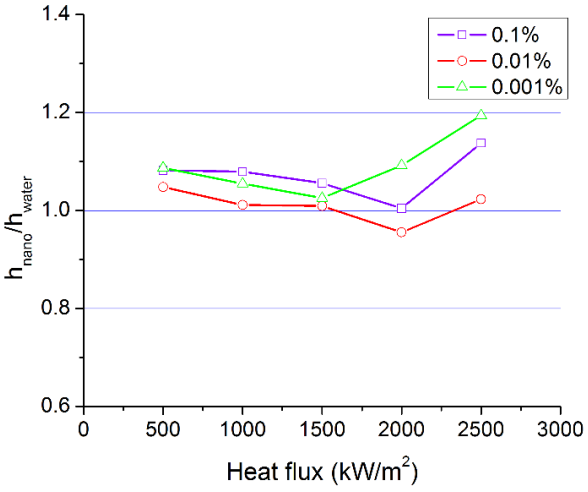

Figure 134: h_{nano}/h_{water} for inlet velocity = 2.5 m/s.(Experimental)

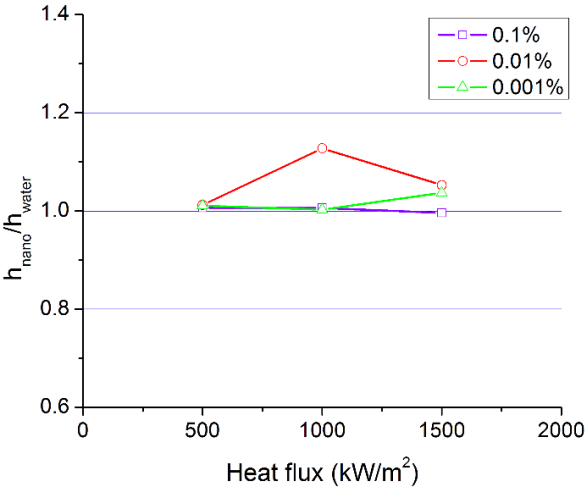

Figure 14: h_{nano}/h_{water} for inlet velocity = 2.0 m/s.(Numerical)

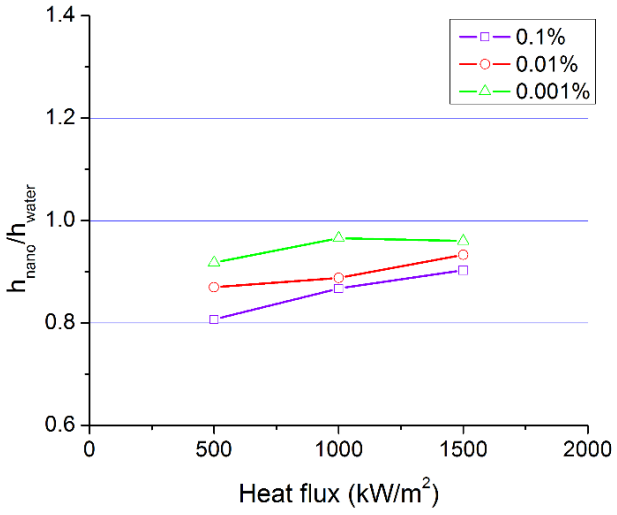

Figure 16: h_{nano}/h_{water} for inlet velocity = 2.0 m/s.(Experimental)

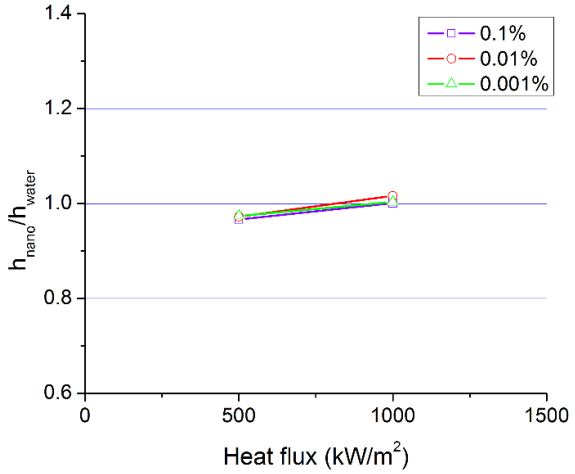

Figure 17: h_{nano}/h_{water} for inlet velocity = 1.5m/s.(Numerical)

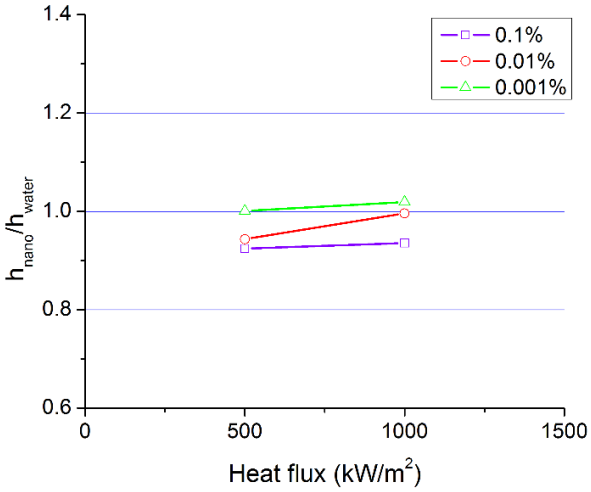

Figure 18: h_{nano}/h_{water} for inlet velocity = 1.5m/s.(Experimental)

Conclusions

In the Eulerian multiphase model, it was observed from the results of the flow boiling of water that the RPI boiling model predicts the volume fraction of vapor with reasonable accuracy. The heat transfer coefficient was computed using the inlet temperature as the bulk temperature. Using this method, it was observed that the heat transfer coefficient was predicted with reasonable accuracy for inlet velocity of $2.5\,m/s$. However, the heat transfer coefficient is over predicted in case of velocities of $2.0\,m/s$ and $1.5\,m/s$. Such behavior can be attributed to the fact that at lower velocities of $2.0\,m/s$ and $1.5\,m/s$ taking the bulk temperature to be inlet temperature was not an accurate assumption due to higher bulk temperature at lower velocities. The RPI model predicts the heat transfer characteristics quickly (lesser computational time). However, formation of nano-particle sublayer and fouling factor is kind of negligible as nanofluid

concentration is very small 0.1%, 0.01% and 0.001% by volume.

References

H. Demir, A. Dalkilic, N. Kürekci, W. Duangthongsuk, S. Wongwises (2011), Numerical investigation on the single phase forced convection heat transfer characteristics of TiO 2 nanofluids in a double-tube counter flow heat exchanger, International Communications in Heat and Mass Transfer, 38, 218-228.

M. Corcione (2011), Empirical correlating equations for predicting the effective thermal conductivity and dynamic viscosity of nanofluids, Energy Conversion and Management, 52, 789-793

C. Tso, C.Y. Chao (2015), Study of enthalpy of evaporation, saturated vapor pressure and evaporation rate of aqueous nanofluids, International Journal of Heat and Mass Transfer, 84, 931-941.

S.J. Kim, T. McKrell, J. Buongiorno, L.-w. Hu, Subcooled flow boiling heat transfer of dilute alumina, zinc oxide, and diamond nanofluids at atmospheric pressure, Nuclear Engineering and Design, 240 (2010) 1186-1194.

T.-H. Lee, R. Situ, T. Hibiki, H.-S. Park, M. Ishii, M. Mori (2009), Axial developments of interfacial area and void concentration profiles in subcooled boiling flow of water, International Journal of Heat and Mass Transfer, 52, 473-487.

H. Abarajith, V. Dhir (2002), A numerical study of the effect of contact angle on the dynamics of a single bubble during pool boiling, in: ASME 2002 International Mechanical Engineering Congress and Exposition, American Society of Mechanical Engineers, pp. 467-475.

X. Li, R. Wang, R. Huang, Y. Shi (2006), Numerical investigation of boiling flow of nitrogen in a vertical tube using the two-fluid model, Applied Thermal Engineering, 26, 2425-2432.

B. Končar, B. Mavko, Modelling of low-pressure subcooled flow boiling using the RELAP5 code, Nuclear Engineering and Design, 220 (2003) 255-273.

J. Tu, G. Yeoh ((2002)), On numerical modelling of low-pressure subcooled boiling flows, International Journal of Heat and Mass Transfer, 45, 1197-1209.

E. Abedini, A. Behzadmehr, S. Sarvari, S. Mansouri (2013), Numerical investigation of subcooled flow boiling of a nanofluid, International journal of thermal sciences, 64, 232-239.

H. Aminfar, M. Mohammadpourfard, M. Sahraro (2012), Numerical simulation of nucleate pool boiling on the horizontal surface for nano-fluid using wall heat flux partitioning method, Computers & Fluids, 66, 29-38.

M. Flows, Theory Guide, ANSYS FLUENT, 14.

N. Kurul, M. Podowski (1991), On the modeling of multidimensional effects in boiling channels, in: ANS Proceeding of the 27th National Heat Transfer Conference.

V.H. Del Valle, D. Kenning (1985), Subcooled flow boiling at high heat flux, International Journal of Heat and Mass Transfer, 28, 1907-1920.

R. Cole (1960), A photographic study of pool boiling in the region of the critical heat flux, AIChE Journal, 6, 533-538.

M. Lemmert, J. Chawla (1977), Influence of flow velocity on surface boiling heat transfer coefficient, Heat Transfer in Boiling, 237, 247.

V. Tolubinsky, D. Kostanchuk, Vapour bubbles growth rate and heat transfer intensity at subcooled water boiling, in: Proceedings of the 4th international heat transfer conference, 1970.

L. Schiller, Z. Naumann, A drag coefficient correlation, Vdi Zeitung, 77 (1935) 51.

F. Moraga, F. Bonetto, R. Lahey (1999), Lateral forces on spheres in turbulent uniform shear flow, International Journal of Multiphase Flow, 25, 1321-1372.

C. Simonin, P. Viollet (1990), Predictions of an oxygen droplet pulverization in a compressible subsonic coflowing hydrogen flow, Numerical Methods for Multiphase Flows, FED91, 65-82.

W. Ranz, W. Marshall (1952), Evaporation from drops, Chemical Engineering Progress, 48, 141446.

J. Laviéville, E. Quémérais, M. Boucker, L. Maas (2005), NEPTUNE CFD V1. 0 User Guide, EDF R&D Chatou.

A. Troshko, Y. Hassan (2001), A two-equation turbulence model of turbulent bubbly flows, International Journal of Multiphase Flow, 27, 1965-2000.

S.E.B. Maïga, C.T. Nguyen, N. Galanis, G. Roy (2004), Heat transfer behaviours of nanofluids in a uniformly heated tube, Superlattices and Microstructures, 35, 543-557.

H. Brinkman (1952), The viscosity of concentrated suspensions and solutions, The Journal of Chemical Physics, 20, 571-571

J.C. Maxwell (1881), A treatise on electricity and magnetism, Clarendon press.

J. Koo, C. Kleinstreuer (2004), A new thermal conductivity model for nanofluids, Journal of Nanoparticle Research, 6, 577-588.

N. Vargaftik, B. Volkov, L. Voljak (1983), International tables of the surface tension of water, Journal of Physical and Chemical Reference Data, 12, 817-820.

S. Cheung, S. Vahaji, G. Yeoh, J. Tu (2014), Modeling subcooled flow boiling in vertical channels at low pressures–Part 1: Assessment of empirical correlations, International Journal of Heat and Mass Transfer, 75, 736-753.